

archives
of thermodynamics

Vol. 42(2021), No. 4, 261–279

DOI: 10.24425/ather.2021.139662

Investigations of thermal-flow characteristics of minichannel evaporator of air heat pump

MICHAŁ JAN KOWALCZYK*
MARCIN ŁĘCKI
ARTUR ROMANIAK
BARTOSZ WARWAS
ARTUR GUTKOWSKI

Lodz University of Technology, Institute of Turbomachinery,
Wólczańska 217/221, 93-005 Łódź, Poland

Abstract The results of experimental investigations of heat transfer and a friction factor in an air channel of the minichannel heat exchanger are presented. The main aim of the analysis was to examine an influence of geometrical parameters of the fin shape with two geometries on heat transfer and flow characteristics of the air channel. The test rig was designed to monitor the parameters of the airflow during cooling by the minichannel heat exchanger. The analysis was conducted with the airflow in the range of 1–5 m/s. The temperature of the evaporation in a refrigeration system was set at 288.15 K. The energy balance of the refrigeration system was carried out. A numerical model describes the airflow through a part of the heat exchanger. Numerical simulations were validated with the experimental data. Numerical methods were used to evaluate the performance of the system and possibilities to improve the fin geometry. The characteristics of the friction factor (a measure of the pressure loss in the airflow) and the Colburn j -factor (heat transfer performance) were calculated. For the maximal velocity of the airflow, the Colburn factor was equal to 0.048 and the evaporator capacity equaled 1914 W.

Keywords: CFD; Numerical methods; Heat exchanger; Minichannel; Louvered fin

*Corresponding Author. Email: michal.kowalczyk.1@dokt.p.lodz.pl

Nomenclature

A	–	airside area of the heat exchanger, m^2
A_c	–	minimal free flow area, m^2
c_p	–	specific heat, $\text{J}/(\text{kgK})$
F_h	–	fin height, mm
F_p	–	fin pitch, mm
f	–	friction factor
h	–	heat transfer coefficient, $\text{W}/(\text{m}^2\text{K})$
j	–	Colburn factor
L_a	–	louver angle, $^\circ$
L_p	–	louver pitch, mm
M	–	air molar mass, kg/mol
MCHE	–	minichannel heat exchanger
n	–	fan rotation frequency, Hz
p	–	pressure, Pa
Δp	–	pressure drop in the MCHE, Pa
Pr	–	Prandtl number
Q	–	heat transfer rate, W
$Q_{\text{ev.air}}$	–	evaporator capacity (airside), W
Re	–	Reynolds number
ΔT_{ln}	–	logarithmic mean temperature difference, K
$T_{\text{ave.inlet}}$	–	average value of temperature upstream of the heat exchanger, K
$T_{\text{ave.outlet}}$	–	average value of temperature downstream of the heat exchanger, K
v_{ave}	–	average velocity, m/s
ν	–	kinematic viscosity, m^2/s
Y^+	–	dimensionless wall distance

Greek symbols

η	–	surface efficiency
μ	–	air dynamic viscosity, $\text{kg}/(\text{m} \cdot \text{s})$
ρ	–	air density, kg/m^3

1 Introduction

Nowadays, minichannel heat exchangers (MCHEs) have become more and more popular. MCHEs reduce the refrigerant load and improve the cooling capacity in comparison to standard heat exchangers. It is possible by replacing a round tube by flat tubes with minichannels. This solution improves the phase change heat transfer coefficient and reduces the airside pressure drop. MCHEs are completely made of aluminum, which reduces their weight.

The MCHE with various parameters of fins was a subject of heat and mass transfer investigations. Islam *et al.* [1] dealt with a review of the heat

transfer enhancement provided by a louvered fin. They analyzed an improvement in heat transfer obtained by changing the geometric parameters of louver fins, which they found in the literature, to show that the alteration could improve the heat transfer by 18% as regards the basic geometry. Muszyński and Koziel conducted a two-dimensional numerical analysis to determine the thermal flow characteristics of the MCHE evaporator during the laminar flow [2]. The investigations covered 363 cases of different geometries, for which an effect of spacing, an angle and a number of louvers on the heat transfer and pressure drop was checked. The highest efficiency was achieved at the 16° angle of the louver inclination. Dodiya *et al.* in [3] presented a comprehensive review of louvered fins in compact heat exchangers. The study showed that louvers applied to fins provided the most encouraging thermal-hydraulic performance. Additionally, they defined the most important parameters that influenced the performance, namely: louver length, louver pitch, flow depth, flow pitch, and fin thickness. In [4], Rui Wan *et al.* investigated experimentally an automotive louvered fin and a flat tube heat exchanger. The investigations were carried on a low-pressure wind tunnel test rig. The presented results showed that the gauge pressure influenced positively the heat exchanger performance. With the gauge pressure of -44 kPa, the airside convective heat transfer coefficient was reduced from 33.5% to 23.3% when compared to 0 kPa. Moreover, they observed a 36.8% increase in the average value of the Colburn j -factor and an increase in the average value of the f factor by 51.2%. Gunnasegran *et al.* [5] studied the effects of geometrical parameters of the louver angle and the fin pitch on the airflow. They carried out 3D numerical investigations using three different fin pitches (1, 2, and 4 mm) and changed louver angles ($+2^\circ$, $+4^\circ$, -2° , -4°) starting from 20° . The simulations were conducted for the Reynolds number in the range 100–1000. A similar investigation was conducted by Djamel *et al.* [6] but only for various louver angles (22° , 25.5° , and 29°). Amirnordin *et al.* [7] conducted 3D numerical simulations to study an effect of the fin geometry on the pressure drop and heat transfer characteristics. The investigations were carried out for the Reynolds number from 200 to 1000 based on the louver pitch. The results showed a good agreement with the experiment (12%) and a relative increase in the heat transfer with an increase in the louver pitch. Chan and Jun investigated an airside pressure drop and heat transfer performance of the louver fin-tube heat exchanger for automobile applications [8]. They carried out experimental and numerical investigations on fourteen louver geometries with different louver pitches and angles. They determined the j and f factors correlations, which were expressed as functions of the average louver pitch, fin pitch, and louver

angle. The presented correlations of heat transfer and pressure drop well agreed with the experiment. Okbaz *et al.* [9] showed numerically a heat transfer improvement and the corresponding pressure drop depending on louver angles between 20° – 30° , the louver pitch 3.8 mm, and the frontal velocity in the range of 1.22–3 m/s.

Park *et al.* [10] carried out the experiment during frosting and defrosting cycles while varying the louver heat exchanger inclination angles (0° , 15° , 30° , and 45°). For larger inclination angles, they observed that the heat transfer rate and the pressure drop varied less during repeated cycles. The use of high inclination angles improved the drainage performance by reducing the mass of its residual water at the same time. Liu *et al.* [11] investigated an effect of operating parameters on the heat transfer performance of a minichannel heat exchanger applied as a cooler. The experiment was conducted under a wide range of MCHE working conditions using the water-cooling method. They found that the optimal air velocity was 2.5 m/s in terms of the heat transfer rate and the airside heat transfer coefficient of the MCHE. They found that the heat transfer rate and the overall heat transfer coefficient increased as the air velocity increased from 1.5 to 2.5 m/s and decreased above 2.5 m/s. Saleem *et al.* [12] performed a systematic numerical study to analyze the airside thermal-hydraulic characteristics. The simulations were conducted in the range of Re from 30 to 500. The geometries were multi-louvered aluminum fins. The investigations were also performed for 36 heat exchanger configurations with the louver angles: 19° – 31° ; the fin pitches: 1.0, 1.2, and 1.4 mm, and the flow depths: 16, 20, and 24 mm. They reported the highest airside heat transfer coefficient and determined a value of the critical Reynolds number. Bohdal *et al.* [13] performed experimental tests to determine the heat transfer during condensation of R134a, R404A, and R407C inside pipes with the internal diameters of 0.31–3.30 mm. The authors obtained local heat transfer coefficients and compared them to the correlations proposed by other researchers. They also proposed their empirical correlation, for which the experimental results fell within $\pm 25\%$.

The present paper attempts to investigate the problem of air channel heat transfer and a friction factor in a minichannel heat exchanger with louver fins. On the basis of the experimental results, values of the j and f factors were determined. The tests were performed for numerical simulation results falling in the range of air velocity of 1–5 m/s. A design of the test rig and results of the numerical simulations are presented in detail. The main goal is to compare the experimental investigations to a numerical model of the minichannel heat exchanger and to examine an influence of geometrical

parameters of the fin shape with two geometries on heat transfer and flow characteristics of the air channel.

2 Materials and methods

2.1 Test rig

The subject of the study is a Danfoss 021U0080 minichannel heat exchanger with rectangular louvered fins. A photo of the MCHE is shown in Fig. 1. The test rig was built according to the ASHRAE 41.2 [14] standard. It consists of two main parts, which are airflow and refrigeration systems. A 3D diagram of the test rig is presented in Fig. 2.



Figure 1: Minichannel heat exchanger under testing.

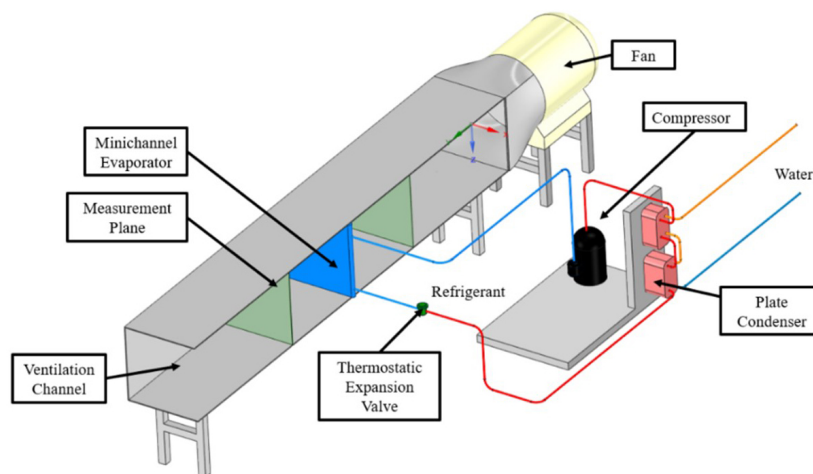


Figure 2: 3D diagram of the test rig.

2.1.1 Airflow system

The rig was designed and built according to the recommendations of the ASHRAE 41.2 standard. The tested heat exchanger was placed inside the airflow channel. The airflow was forced by a fan located at one end of the channel, which drew in the air. According to the ASHRAE standard, the channel was divided into a few sections, including measurement sections, a straightener section, a mixing section, etc.

The ASHRAE standard specifies relative lengths of the channels. The channel cross-sections had to be adjusted to dimensions of the tested heat exchanger (and the fan inlet diameter). Having analyzed the above-mentioned factors, a 300 mm × 300 mm cross-section was selected in the front of the heat exchanger and 330 mm × 330 mm behind it (fan diameter: 400 mm). The total length of the airflow duct was equal to 7.046 m.

The fan had to ensure the airflow range equivalent to the velocities span found in air-conditioning and cooling systems (0.5–4.5 m/s). Accordingly, the fan had to overcome a pressure drop of the air flowing through the channel. Based on this, Soler & Palau TD 6000/400 axial fan was selected. The maximal average velocity obtained for the highest rotational fan speed (50 Hz) was 5.2 m/s. A Toshiba VF-S15 inverter was used to control the fan rotational speed.

On the basis of the ASHRAE standard, the air velocity was measured in the plane upstream of the heat exchanger at the distance of about 15 cm at 25 points according to the Log-Chebyshev method. The LB580 climate meter was used to measure the air velocity – the measurement error was ± 0.05 m/s (+3% of the measured value). It was also decided to install two grids on which T-type thermocouples were placed to obtain an average airstream temperature. Their distribution was determined with the Log-Chebyshev method (temperature measurement at the same points as the velocity measurement) [14]. The thermocouple measurement error was established on the basis of an earlier calibration of thermocouples at the level of ± 0.2 K. Static pressure should be measured in four taps according to the ASHRAE standard. A CHY 386P digital manometer was used to measure a static pressure drop through the heat exchanger. The meter accuracy was of ± 6 Pa. The measurement data acquisition system for the rig was based on the National Instruments CompactRIO chassis with modules. In Fig. 3, a schematic arrangement of the measurement data acquisition system is shown. The results obtained from the experiment are presented in Table 1.

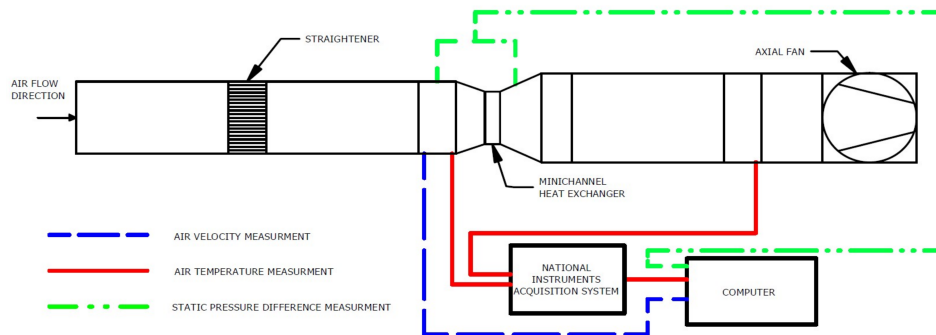


Figure 3: Schematic block diagram of the measurement data acquisition system.

Table 1: Measurement results for the Danfoss minichannel exchanger.

No.	n	v_{ave}	$T_{ave.inlet}$	$T_{ave.outlet}$	$Q_{ev.air}$	Δp
	(Hz)	(m/s)	(K)	(K)	(W)	(Pa)
1	13.0	1.17	300.25	292.55	944	12.7
2	18.5	1.99	299.35	293.55	1224	32.3
3	25.0	3.07	300.05	294.95	1626	44.0
4	31.0	3.88	299.85	295.65	1698	71.4
5	35.0	4.58	299.75	295.75	1914	84.1

Prior to the measurements, the air relative humidity, which did not exceed 40% for an ambient temperature of 300.15 K, was measured by Lab-El LB580 climate meter with uncertainty $\pm 2\%$. Under those conditions, the dew point temperature was 285.40 K. The evaporation temperature was set at 288.15 K, so the condensation did not occur during the tests.

2.1.2 Refrigeration system

The refrigeration system enables most important thermodynamic parameters of the refrigerant to be measured at the points indicated in Fig. 4 (1–4). It consists of a scroll compressor (the power of which is controlled with a frequency converter), a water-cooled plate heat exchanger (which is a condenser), a thermostatic expansion valve, and a minichannel heat exchanger (which is an evaporator) to be tested. The temperature and pressure measurement was carried out with T-type thermocouples and Danfoss gauge pressure transducers. The National Instrument CompactRIO with suitable C series modules was used as a data acquisition system with the

LabView software. A list of the most important elements of the refrigeration system is presented in Table 2.

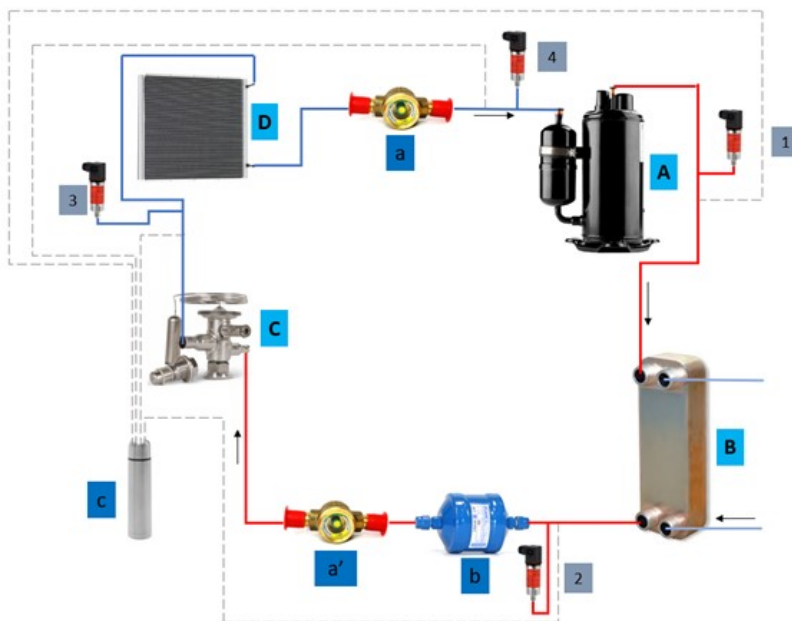


Figure 4: Scheme of the refrigeration system of the test rig.

Table 2: List of the refrigeration system components.

Symbol	Type	Parameter	Operating rate	Uncertainty
A	Scroll compressor GMCC DA110S1C-30FZ	Refrigeration capacity (W)	0–5200	–
B	Condenser Secespol RA14-10	Power range (W)	500–4000	–
C	Expansion valve Danfoss 068U1714	Power range (W)	500–2500	–
D	Minichannel heat exchanger Danfoss 021U0080	Power range (W)	500–2500	–
a, a'	Sight glasses GAR SPU	–	–	–
b	Filter drier Castel 4316/3S	–	–	–
c	Vacuum Flask	–	–	–
1, 2, 3, 4	Pressure transmitters Danfoss AKS 33	Pressure (kPa)	–100–3100	± 10.4 kPa
1, 2, 3, 4	Type T thermocouples Omega	Temperature (K)	73.15–573.15	± 0.2 K

The following refrigeration system parts were thermally balanced:

- a condenser – by measurement of operating parameters of the refrigerant and the cooling water,
- an evaporator – by measurement of operating parameters of the refrigerant and the airflow.

Figure 5 presents the experimental results for the cooling capacity of the heat exchanger from the air and refrigerant flow sides. The experiment was carried out at 1–5 m/s of the average velocity span.

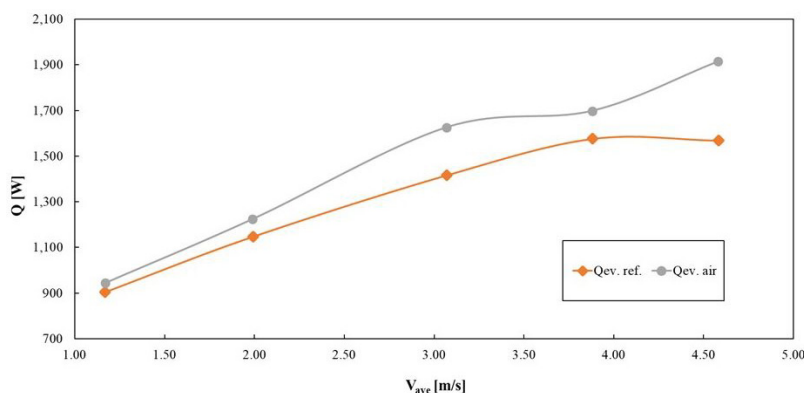


Figure 5: Cooling capacity of the MCHE measured at the air and refrigerant side *versus* the average flow velocity.

2.2 Numerical model

The computational model was based on the tested MCHE geometry (Fig. 1). A schematic drawing with main dimensions was prepared for this purpose. Considering the repeatability of the fin structure and in order to save the computational power, the simulations were made for a MCHE segment as shown in Fig. 6.

Geometrical models for the simulations were prepared in SpaceClaim 2020 R2. A 3D model of the MCHE segment was built from a fragment of the fin and two flat tubes of half thickness. The first model was prepared with plain fins and the second one was equipped with louvers. Both models are shown in Fig. 7. The geometrical parameters of the fins were set as: fin height $F_h = 8$ mm, fin pitch $F_p = 1$ mm. In case of second geometry, louver angle set as $L_a = 20^\circ$ and louver pitch set as $L_p = 0.96$ mm.

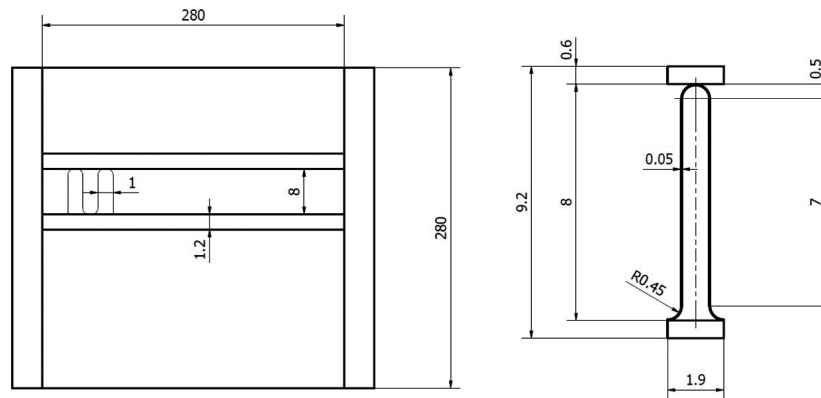


Figure 6: Schematic drawing with main dimensions (in mm) and a model of the segment used in the simulations.



Figure 7: Geometrical model: plain fin (left picture) and louvered fin (right picture).

The numerical investigations involved two domains. The fluid domain was defined as air at 298.15 K and the solid domain was defined as aluminum. The thermophysical parameters of air and aluminum are presented in Table 3.

The mesh was generated to model accurately heat transfer phenomena in high temperature and velocity gradient areas. A number of elements grew in the area of louvered fins. In the area of louvered fins, a triangular mesh was generated, whereas a hexagonal mesh was applied to reduce the number of elements in the regions upstream of the inlet and downstream of the outlet. The statistics of the mesh was: 875,957 nodes and 2,495,113 elements. The average value of the aspect ratio was under 100 and the minimal corner angle was 61° . A view of the fluid and solid domain mesh is depicted in Fig. 8.

Table 3: Thermodynamical parameters from the numerical simulations.

Parameter	Air molar mass	Air density	Air specific heat	Pressure	Air dynamic viscosity	Air thermal conductivity	Aluminum thermal conductivity
Unit	$\frac{\text{kg}}{\text{kmol}}$	$\frac{\text{kg}}{\text{m}^3}$	$\frac{\text{J}}{\text{kg} \cdot \text{K}}$	Pa	$\frac{\text{kg}}{\text{m} \cdot \text{s}}$	$\frac{\text{W}}{\text{m} \cdot \text{K}}$	$\frac{\text{W}}{\text{m} \cdot \text{K}}$
Value	28.96	1.185	1004	101325	1.831×10^{-5}	2.61×10^{-2}	237

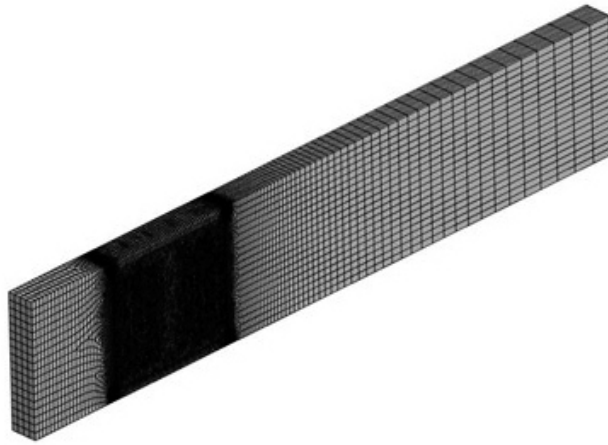


Figure 8: View of the computational mesh.

Numerical investigations were conducted for five inlet velocities (from 1 to 5 m/s, with a step of 1 m/s). A constant velocity boundary at the inlet was set up. An outlet boundary was 0 Pa relative pressure. In the horizontal direction, a transitional periodicity was set. Additionally, a symmetry boundary was applied on the walls and interfaces at contact areas of the two domains. The refrigerant side was included as an area of the constant temperature equal to 288.15 K, which is the evaporation temperature in the heat pump refrigeration system. All boundary conditions are shown in Fig. 9.

The simulations were conducted in Ansys CFX 2020 R2 [15] with the model of turbulence set as a SST $k-\omega$ model. The convergence criteria for the momentum and heat transfer were 10^{-6} . The investigations were conducted for two geometries: simplified fins without louvers and an enhanced fin model with louvers. This approach was also applied in [16]. The maximal value of Y^+ for the velocity of 5 m/s was close to 6.

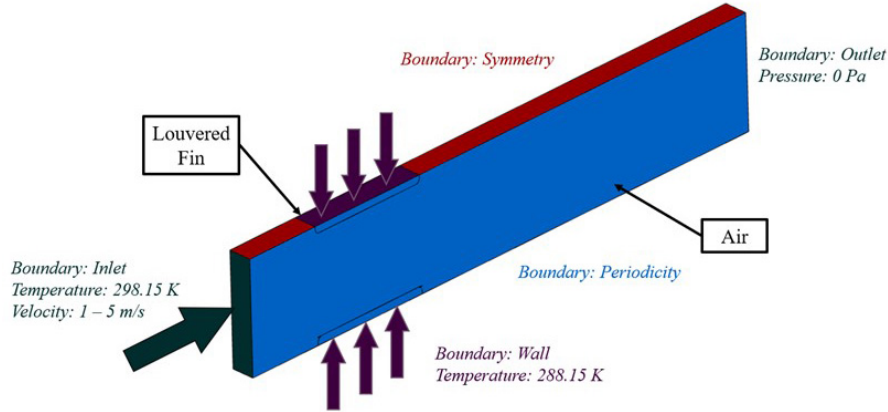


Figure 9: Boundary conditions used in the simulations.

3 Results

The experimental results presented in Fig. 10–13 refer to the tested Danfoss minichannel heat exchanger, which has louvered fins modeled in the numerical simulations. The simulation outcomes were used to determine the characteristics of a pressure drop and a cooling effect (a temperature difference between the inlet and outlet of the louvered fin heat exchanger) with respect to the flow velocity. A validation of the simulations was conducted on the basis of the experimental results. A comparison of the pressure and temperature drop characteristics for the numerical simulations and the experiment is presented in Figs. 10 and 11.

The heat transfer and pressure drop characteristics are also reduced to the form of Colburn and friction factors [17]. The calculations were conducted according to the formulas shown in following equations:

$$\text{Re} = \frac{v_{\text{ave}} L_p}{\nu}, \quad (1)$$

$$f = \frac{2\Delta p}{\rho v_{\text{ave}}^2} \frac{A_c}{A}, \quad (2)$$

$$j = \frac{\eta h \text{Pr}^{\frac{2}{3}}}{\rho v_{\text{ave}} c_p}, \quad (3)$$

$$h = \frac{Q}{A \Delta T_{\text{ln}}}. \quad (4)$$

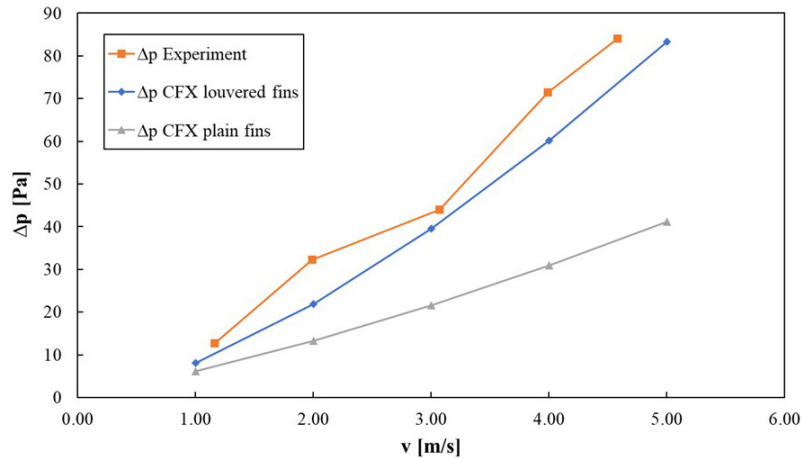


Figure 10: Comparison of the pressure drop characteristics.

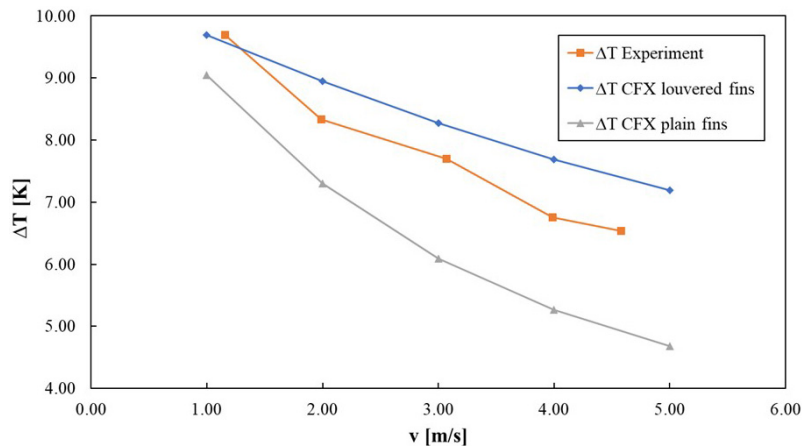


Figure 11: Comparison of the cooling effect characteristics.

As regards the experiment, the values measured at the test rig were used in the formulas. However, in the case of the numerical simulations, the values were obtained from the postprocessing stage of the simulations (Ansys CFD-POST 2020 R2). These parameters were: the differences in pressure at the inlet and outlet from the domain, the average velocity in the air domain, and wall and air temperatures. In case of j -factor formula, the surface efficiency coefficient was included. The surface efficiency coefficient determine the decreasing of heat transfer area due to real fin efficiency.

In studied case the value of surface efficiency was $\eta = 0.99$. The calculated values of the factors f and j in relation to the Reynolds number are shown in Figs. 12 and 13.

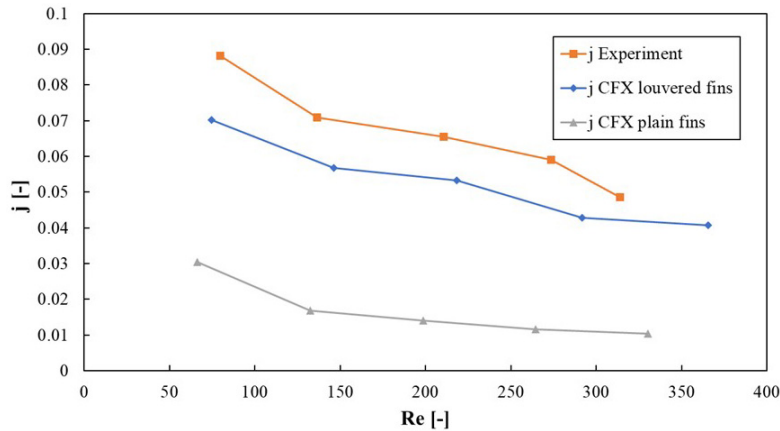


Figure 12: Heat transfer characteristics in a dimensionless form.

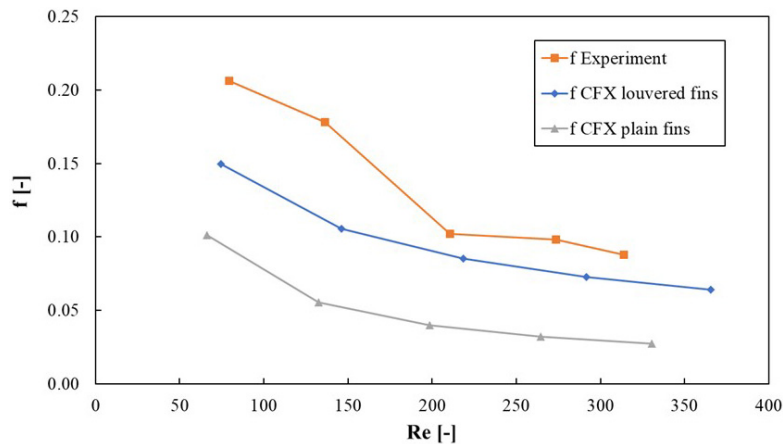


Figure 13: Pressure drop characteristics in a dimensionless form.

A contour plot of the velocity distribution with vectors is shown in Fig. 14. Both tested geometries were presented to show significant differences in the flow behavior. Contours of the air temperature distribution as it flows through both geometries are shown in Fig. 15. A total pressure distribution for the tested geometries is presented in Fig. 16. This aspect is important in terms of flow resistance.

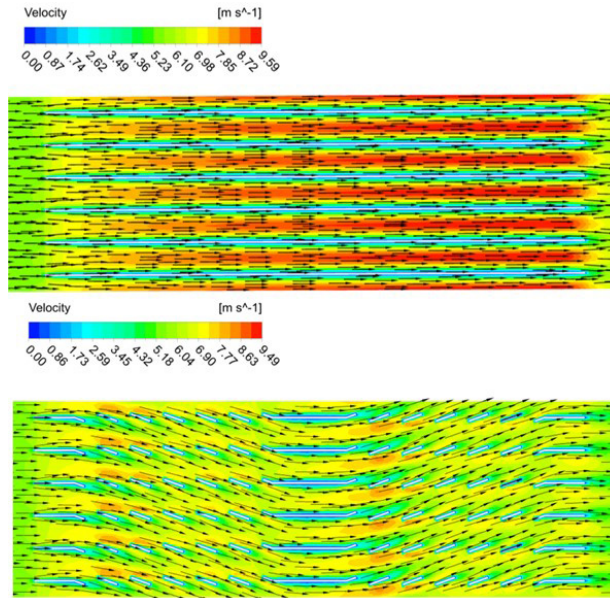


Figure 14: Velocity distribution with vectors: plain fin (top picture); louvered fin (bottom picture).

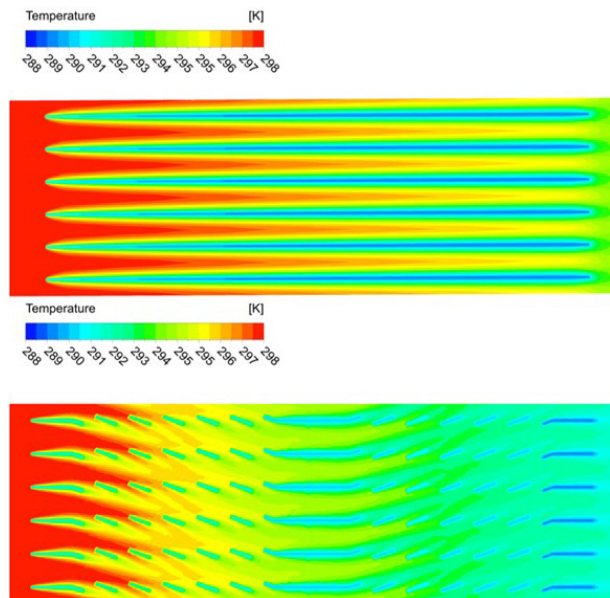


Figure 15: Temperature distribution: plain fin (top picture); louvered fin (bottom picture).

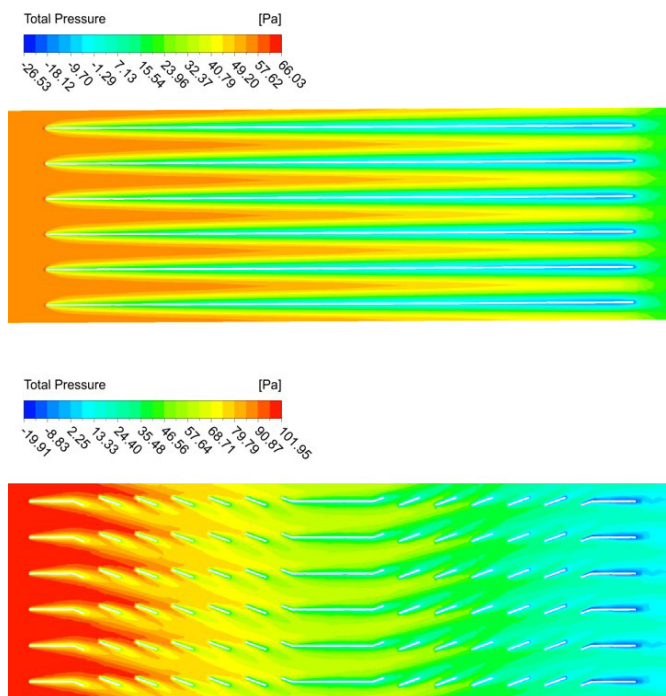


Figure 16: Total pressure distribution: plain fin (top picture); louvered fin (bottom picture).

4 Discussion

The discrepancies between the heat transfer rates from the experiment and the simulations visible in Fig. 5 are in the range of 4–22%, where the highest difference was recorded for the highest airflow velocity. This high-value discrepancy results from a lack of the mixing plate downstream of the exchanger in the measuring channel, which would ensure a uniform temperature distribution at the second temperature measurement plane. An additional limitation was a thermostatic expansion valve, which increased the steam superheat in the evaporator as the air velocity increased, which enlarged the non-uniformity of the temperature profile.

The characteristics obtained from the experiment and the numerical simulations presented in Figs. 10 and 11 exhibit similar trends. For the pressure drop characteristics, the discrepancies for louvered fins between the experiment and the simulation are in the range of 1–36%. The pressure drop increases at a higher velocity. In the case of the cooling effect, the temper-

ature differences between the inlet and outlet decrease with an increase in velocity. The highest difference between the experiment and the louvered fin simulations is equal to 14%. An addition of louvers in the plain fin model increased the pressure drop to the values twice as high and improved the heat transfer in the range of 7–54%.

The differences between the experiment and simulation results can follow from a mechanical deformation of the heat exchanger fins, which are very thin and prone to mechanical damage. It causes differences in the shape of lamellas in the whole heat exchanger, which the model does not cover. Additionally, the aforementioned deformations affect the angle of the louver, which is fixed as a constant value in the simulation.

According to the j and f characteristics, there are differences between the experimental results and the numerical solutions in Figs. 12 and 13. Both factors (j and f) values are lower for the numerical simulations than from the experiment. The Colburn factor j for both methods has a similar tendency. The discrepancies between the experiment and the simulation for louvered fins are in the range of 16–28%. The differences between plain fins and louvered fins are in the range of 131–296%. In the case of friction factor values, one can observe a better agreement for higher values of the Reynolds number. For Reynolds numbers above 200, the discrepancies between the experiment and the simulation for louvered fins are in the range of 28–41%. The friction factor values for louvered fins are even twice as high as for plain fins.

The distribution of flow velocity shows that the maximal value of velocity is twice as high as its value at the inlet. The acceleration area can be observed in the flow at the inlet and half-length of the fins. The louvered fins direct the flow in the next row of fins (secondary flow), which can be seen in Fig. 14, where a straight-line flow can be observed with plain fins. The temperature distribution (Fig. 15) shows a linear temperature drop along the plain fin. For the louvered fin, a significantly greater temperature drop was visible, reaching the difference of 5 K at the outlet relative to the plain fin. It can be observed that the influence of the louvers on the creation of secondary flow affects the disturbance of the boundary layer flow, intensifying the heat transfer. The total pressure distribution (Fig. 16) shows an even pressure drop along the plain fin. In the case of a louvered fin, zones of low pressure can be observed near the end of the fins, which were caused by the boundary layer separation. The secondary flow, which changes the direction of the airflow to the center section of the fin, disrupts the formation of the boundary layer.

5 Conclusions

The experiment was conducted following the ANSI ASHRAE standard, for new operating conditions of a small refrigeration system (e.g., the evaporation temperature of 288.15 K), where the maximal value of cooling capacity of 1,914 W was achieved. A minichannel heat exchanger with specific dimensions 280×280 mm was subject to investigation. A numerical model of the tested minichannel heat exchangers was generated and it contained louvered fins and plain fins. An influence of louvers on operation of the heat exchanger was examined, including an analysis from the heat transfer and flow side (j and f factors). A good agreement of the numerical model of heat transfer was achieved for the louvered heat exchanger in the range up to 14%.

Acknowledgement This article has been completed while the first, third, and fourth authors were Doctoral Candidates in the Interdisciplinary Doctoral School at the Lodz University of Technology, Poland. We would like to thank Malgorzata Jozwik for her significant linguistic help during the preparation of the manuscript.

Received 6 November 2021

References

- [1] ISLAM S., ISLAM M.S., ABEDIN M.Z.: *Review on heat transfer enhancement by louvered fin*. Int. J. Eng. Mater. Manufact. **6**(2021), 60–80.
- [2] MUSZYŃSKI T., KOZIEL S.M.: *Parametric study of fluid flow and heat transfer over louvered fins of air heat pump evaporator*. Arch. Thermodyn. **37**(2016), 3, 45–62.
- [3] DODIYA K., BHATT N., LAI F.: *Louvered fin compact heat exchanger: a comprehensive review*. Int. J. Amb. Energ. (2020).
- [4] WAN R., WANG Y., KAVTARADZE R., JI H., HE X.: *Research on the air-side thermal hydraulic performance of louvered fin and flat tube heat exchangers under low-pressure environment*. Exp. Heat Transfer **33**(2020), 1, 81–99.
- [5] GUNNASEGARAN P., SHUAIB N.H., ABDUL JALAL M.F.: *The effect of geometrical parameters on heat transfer characteristics of compact heat exchanger with louvered fins*. ISRN Thermodyn. (2012), 1–10.
- [6] DJAMAL H.D., WOON Q.Y., SUZAIRIN M.S., HISHAM AMIRNORDIN S.: *Effects of geometrical parameters to the performance of louvered fin heat exchangers*. Appl. Mech. Mater. **773-774**(2015), 398–402.

- [7] AMIRNORDIN S.H., DIDANE H.D., NORANI MANSOR M., KHALID A, SUZAIRIN M.S., RAGHAVAN V.R.: *Pressure drop and heat transfer characteristics of lowered fin heat exchangers*. Appl. Mech. Mater. **465-466**(2014), 500–504.
- [8] CHAN KANG H., JUN G.W.: *Heat transfer and flow resistance characteristics of lower fin geometry for automobile applications*. J. Heat Transfer. **133**(2011), 1–6.
- [9] OKBAZ A., OLCAY A.B., CELLEK M.S., PINARBAŞI A.: *Computational investigation of heat transfer and pressure drop in a typical lower fin-and-tube heat exchanger for various lower angles and fin pitches*. EPJ Web Conf. **143**(2017), 02084.
- [10] PARK J.S., KIM J., LEE K.S.: *Thermal and drainage performance of a lowered fin heat exchanger according to heat exchanger inclination angle under frosting and defrosting conditions*. Int. J. Heat Mass Transf. **108**(2017), 1335–1339.
- [11] LIU X., CHEN H., WANG X., AND KEFAYATI G.: *Study on surface condensate water removal and heat transfer performance of a minichannel heat exchanger*. Energies **13**(2020), 5, 1065
- [12] SALEEM A., KIM M.H.: *CFD analysis on the air-side thermal-hydraulic performance of multi-lowered fin heat exchangers at low Reynolds numbers*. Energies **10**(2017), 6, 1–24.
- [13] BOHDAL T., CHARUN H., SIKORA M.: *Heat transfer during condensation of refrigerants in tubular minichannels*. Arch. Thermodyn. **33**(2012), 2, 3–22.
- [14] ASHRAE: ANSI/ASHRAE Standard 41.2-1987: Standard Methods for Air Velocity and Airflow Measurement (2018).
- [15] Manual Ansys-CFX, Release 2020 R2. <http://www.ansys.com> (accessed 15 July 2020).
- [16] JASIŃSKI P.B., KOWALCZYK M.J., ROMANIAK A., WARWAS B., OBIDOWSKI D., GUTKOWSKI A.: *Investigation of thermal-flow characteristics of pipes with helical micro-fins of variable height*. Energies **14**(2021), 8, 2048.
- [17] KANG, HIE-CHAN & JUN, GIL.: *Heat transfer and flow resistance characteristics of lower fin geometry for automobile applications*. J. Heat Transf. **133** (2011), 101802.